

Origin and the role of device physics in the magnetic field effect in organic semiconductor devices

B. K. Li¹, H. T. He¹, W. J. Chen¹, M. K. Lam², K. W. Cheah², and J. N. Wang^{1*}

¹*Department of Physics, Hong Kong University of Science and Technology, Clear Water Bay, Kowloon, Hong Kong, China*

²*Center of Advanced Luminescence Materials, Department of Physics, Hong Kong Baptist University, Kowloon Tong, Hong Kong, China*

*email: phjwang@ust.hk

A small magnetic field (~30 mT) can effectively modulate the electroluminescence, conductance and/or photocurrent of organic semiconductor based devices, up to 10% at room temperature. This organic magnetic field effect (OMFE) is one of the most unusual phenomena of both organic electronics and, more basically, magnetism, since all device components are nonmagnetic. However, in spite of latest surge of research interest, its underlying mechanism is still hotly debated. Here we experimentally identify that the magnetic field induced increase of intersystem crossing rate (between either excitons or polaron pairs), and decrease of triplet exciton-polaron quenching rate are responsible for the observed OMFEs. The diversity of observed OMFE results, such as sign change and operating condition dependence, originates from the difference of devices physics.

Organic semiconductor (OSE) based devices, such as organic light emitting diodes (OLEDs), organic photovoltaic cells and thin film transistors, as well as spintronic devices, have been successfully developed in the past few decades (ref. 1 and 2, and references therein). Although the magnetic field effect on luminescence, photoconductance in organic materials have been studied in the past [3,4], renewed research interest has surged very recently due to the recent discovery that a small magnetic field of ~ 30 mT can effectively modulate the electroluminescence (EL) and/or conductance up to ~10% at room temperature in organic devices, such as OLEDs, organic single layer sandwiched structures and organic photovoltaic devices, without any magnetic materials [5-19]. These organic magnetic field effects (OMFEs) do not possess magnetic field direction dependence. Obviously, the OMFE can be easily used as an external way to further increase the efficiency of organic photovoltaic devices, and to modulate the efficiency of OLEDs. New kinds of devices, such as magnetic sensors [19,21] and OLED based touch-screen devices using the OMFE can also be developed, further enriching the field of OSE applications.

OMFE is a universal phenomenon and has been observed and studied in various polymer and/or small molecular OSEs based devices. However, the observed experiment results were inconsistent and difficult to interpret. Firstly, the sign of OMFE can be positive or negative, depending on material [7], device structure such as layer thickness [14], and also on operating conditions such as applied bias and temperature [7,15]. Secondly, in study of OMFEs, usually only a low field (~30 mT) component, which saturates relatively fast, can be observed, while a high field (>100 mT) component has also been reported by several groups very recently [13,15,16]. Different physical processes, which are believed to be magnetic field dependent, have been proposed as the origin of OMFE, such as intersystem crossing (ISC) between

polaron pairs (PPs) [5,8,9,11,14,20], triplet-triplet annihilation [12,13], polaron scattering by triplet excitons [14], triplet exciton quenching induced by polaron [14,31], influence on charge transfer states (Δg mechanism) in blend structure [15], polaron pair formation [16], mobility change of minority carriers [17], and bipolaron formation [18]. From these physical processes, two kinds of models have been proposed to explain the complexity and divergence of experiment results. One is multi-process based model [14,15], in which it is proposed that different signs and/or different field dependences originate from different physical processes. The other is single-process based model [9,11,17], in which the sign change is a result of secondary effect. For example, the change of singlet/triplet exciton ratio, originating from the magnetic field induced reduction in ISC between PPs, can modulate the device current, either because of the different roles that singlet and triplet excitons plays in conductance [9], or through the change of recombination current [11]. The multi-process models are individual device dependent, while the single-process models do not explain the existence of different magnetic field dependent components. A simple universal model, which can explain not only the sign changes complexity but also the existence of different field dependent components, is lacking.

In this study, we show that magnetic field induced increase in singlet-triplet ISC rate (between either excitons or polaron pairs) and decrease in triplet exciton-polaron quenching rate are responsible for the observed OMFE. Based on these two processes, we show that the variety of observed phenomena, such as the coexistence of low- and high- field components, sign changes, as well as the material dependence, organic layer thickness dependence and operating conditions dependence, of the measured OMFE curves, is result of the change of devices physics.

In this work we used two small molecule OSEs,

N,N' -di(naphthalene-1-yl)- N,N' -diphenyl-benzidine (NPB) and tris-(8-hydroxyquinolato) aluminium (Alq_3), both widely used in OLEDs as hole transport layer and electron transport/emission layer, respectively [22], as active layer in our single layer sandwiched devices, with a structure of ITO/OSE/cathode. One advantage of small molecular over polymer is the higher purity, which can exclude any extrinsic influence of the observed OMFES [1]. Magnetic field effects on photocurrent (MPC) of the devices were systematically studied as a function of photon excitation energy (E_{hv}), applied bias (V), and layer thickness (d). The MPC is defined as:

$$MPC\% = \frac{PC(B) - PC(B=0)}{PC(B=0)} \times 100\% \quad (1)$$

where PC , i.e. photocurrent is the illumination induced device current change.

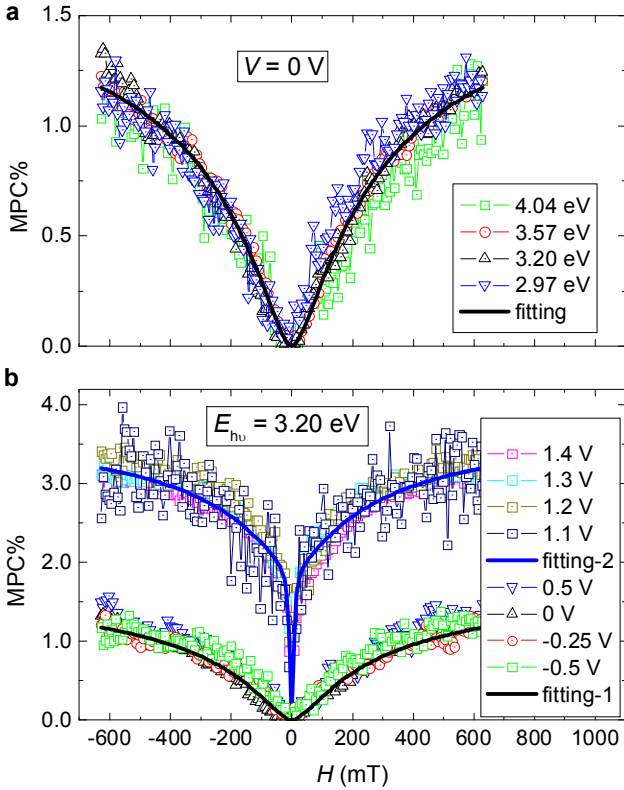


Figure 1 MPC of device ITO/NPB(50 nm)/Al. **a**, MPC curves measured at zero bias with excitation photon energies ranging from 2.94 to 4.04 eV. The solid line is fitting results using empirical equation (2), with $MPC_{\infty} = 1.8$ and $B_{0\text{HF}} \sim 140$ mT, respectively. **b**, MPC curves measured at different bias conditions with fixed excitation photon energy at 3.20 eV. The black solid line is fitting result using equation (2), with $MPC_{\infty} = 1.8$ and $B_{0\text{HF}} \sim 140$ mT. The blue solid line is fitting result using equation (3), with $MPC_{\text{HF}\infty} = 1.8$, $MPC_{\text{LF}\infty} = 2.0$, $B_{0\text{HF}} = 140$ mT and $B_{0\text{LF}} = 8$ mT, respectively.

Figure 1 shows the MPC curves of device D_{N50} , ITO/NPB (50 nm)/Al. The MPC curves measured at different photon excitation energies, with E_{hv} ranging from 2.97 eV to 4.04 eV, under zero bias condition, are shown in Fig. 1(a). Figure 1(b) illustrates the V dependent MPC curves with $E_{\text{hv}} = 3.20$

eV, as V varying from -0.5 V to 1.4 V. As shown in Fig. 1(a), the MPC is positive and does not show significant E_{hv} dependence. The line shape can be fitted by the empirical equation [7],

$$MPC(B) = \frac{MPC_{\infty} \cdot B^2}{(|B| + B_0)^2} \quad (2)$$

with $MPC_{\infty} = 1.8$ and $B_0 = 140$ mT, respectively, where MPC_{∞} is the MPC at an infinite B field and B_0 is the characteristic field width. The fitting result of B_0 , ~ 140 mT, is significantly larger than those reported [7]. We refer this MPC behaviour as the high field (HF) component. While with fixed $E_{\text{hv}} = 3.20$ eV, the V dependent MPC curves can be categorized into two groups, as shown in Fig. 1(b). The line shapes of MPC do not show significant bias dependence. For $V < V_t$, where V_t is the turn-on voltage which approximately is 0.9 V for D_{N50} , the MPC curves can be fitted with the HF component, i.e. using equation (2) with $MPC_{\infty} = 1.8$ and $B_{0\text{HF}} \sim 140$ mT. When $V > V_t$, a new low field (LF) component emerges while the HF component remains unchanged. The MPC curves can be fitted by

$$MPC(B) = \frac{MPC_{\infty\text{HF}} \cdot B^2}{(|B| + B_{0\text{HF}})^2} + \frac{MPC_{\infty\text{LF}} \cdot B^2}{B^2 + B_{0\text{LF}}^2} \quad (3)$$

where the first term is the HF component and the second term is the LF component, with $MPC_{\text{HF}\infty} = 1.8$, $MPC_{\text{LF}\infty} = 2.0$, $B_{0\text{HF}} = 140$ mT and $B_{0\text{LF}} = 8$ mT, respectively. To understand the observed MPC effect, detail analyses of the PC generation mechanism is necessary and identify the prime magnetic field affects.

In rigid band approximation [23], the highest occupied molecular orbital (HOMO) of NPB lies about 0.6 eV below the ITO Fermi level (E_{F}), whereas the lowest unoccupied molecular orbital (LUMO) lies about 1.8 eV above $\text{Al } E_{\text{F}}$ (ref. 24, 25), as shown in Fig. 2(a). Schematic band diagrams of device D_{N50} , under different bias conditions, are shown in Fig. 2(b) and (c). The mechanism of PC generation includes four basic processes: (i) exciton generation. In OSEs, absorption of a photon can only generate singlet excitons (S_{X}), and triplet excitons (T_{X}) will be generated from S_{X} through ISC [26,27]. (ii) exciton diffusion. Since excitons are neutral species, their motions are not influenced by electric field and they diffuse via random hops. In principle, T_{X} has larger diffusion length (> 10 nm) than that of S_{X} (a few nanometers) [27,28]. And in fact, an increasing number of organic solar cells relies on the diffusion of T_{X} to dissociating interface [27, and references therein]. (iii) exciton dissociation. Given the typically large exciton binding energy in NPB and/or Alq_3 , about 1 eV [29], the dissociation of excitons in bulk can be ignored but only occurs at metal-organic interfaces (M/OSE), where an energy compensation, Δ , is available [27,30], as shown in Fig. 2(b) and (c). The number of $S_{\text{X}}/T_{\text{X}}$ diffusing to the M/OSE interfaces actually controls the free carrier generation. The dissociated electrons and holes at M/OSE interface will either annihilate or further separate to become free carriers. The energy compensation Δ plays important role in exciton dissociation, while the electric field

suppresses the annihilation process and benefit the effective dissociation. (iv) carrier transport in OSE. The generated free carriers at M/OSE interface will drift/diffuse, described as polaron hopping from molecular to molecular, towards respective electrodes. The positive/negative polarons will either reach the opposite electrodes or recombines to form PPs, depending on the PP formation rate and the carrier mobility (μ) which determines the carrier transport time through the OSEs.

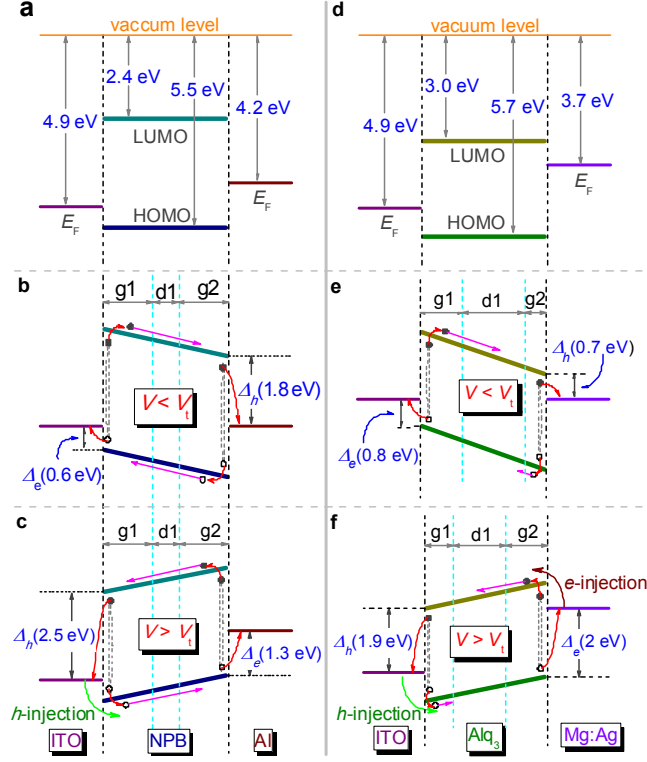
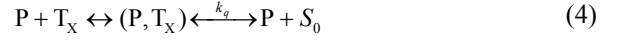


Figure 2 Schematic band diagrams. **a**, The ITO and Al electrodes Fermi levels E_F , and LUMO/HOMO energy levels of NPB. **b**, Band diagram of ITO/NPB(50 nm)/Al (D_{N50}) when $V < V_t$. **c**, Band diagram of D_{N50} when $V > V_t$. **d**, The ITO and Mg:Ag electrodes Fermi levels E_F , and LUMO/HOMO energy levels of Alq₃. **e**, Band diagram of ITO/Alq₃(50 nm)/Mg:Ag (D_{A50}) when $V < V_t$. **f**, Band diagram of D_{A50} when $V > V_t$. Δ represents energy compensation for the exciton dissociations at M/OSE interfaces. In cases of $V < V_t$ and $V > V_t$, Δ for releasing electrons and/or holes are different. Region g1/g2 represents the generation zone, in which the excitons can diffuse to M/OSE interface and contribute to dissociation. Region d1 represents the zone that out of the exciton diffusion length from M/OSE interfaces.

From PC generation processes described above, it can be seen that any magnetic field induced changes of carrier mobility, and/or the number of excitons that can diffuse to M/OSE interface will lead to photocurrent modulation. In our small molecular OSE based sandwiched structures, we consider two processes, both include carrier spin information that are magnetic field dependent. One is the magnetic field induced decrease of P- T_X quenching (TPQ process) [14,31], and another is the magnetic field induced increasing of ISC

rate between singlet and triplet states (ISC process) [26]. TPQ process can be described as



where S_0 is the ground state and k_q is the quenching rate which decreases with increasing magnetic field [14,31]. The left-hand side describes the scattering of polarons by T_X , and this scattering is field independent. Changing of T_X density will result in modulation of photocurrent, because it will either affect the scattering of polarons, altering the polaron mobility, or change the number of excitons that can contribute to dissociation at M/OSE interface. The ISC happens in both among exciton states and PP states, depending on the singlet/triplet generation mechanism. In a photon absorption case, due to the fact that photon excitation can only generate S_X , the ISC translates S_X into T_X . While in a polaron-polaron recombination case, the ISC translates triplet polaron pairs (T_{PP}) into singlet polaron pairs (S_{PP}) due to their density difference (formation ratio is 3:1) and energy degeneracy. But in both cases, the ISC rate k_{ISC} will increase when an external magnetic field applied.

The B field induced increase of k_{ISC} leads to an increment of T_X , consequently inducing a positive MPC component by increasing the total number of excitons that can diffuse to M/OSE interface to dissociate, as well as a negative MPC component by increasing the P- T_X scattering probability to limit polaron mobility. Both the positive and the negative components follow the same B dependence as $k_{ISC}(B)$. The B field induced decrease of k_q , saving more T_X , will also induce both positive and negative MPC effects, following a same B dependence. Obviously, the signs of MPC_{ISC-X} and MPC_{TPQ} should be the same because both originate from the increase of T_X density. The PP formation can be considered as a secondary process, and the increase of S_{PP} , though B field induced increase of k_{ISC-PP} , has a device dependent effect on the MPC. When the values of e/h mobility differ a lot and the PP formation zone locates near one M/OSE interface due to carrier accumulation, the $k_{ISC-PP}(B)$ effect should be considered, otherwise, it can be ignored, as will be discussed later.

The values of e/h mobility in NPB are large and in same order of magnitude [24], $\mu_e \sim \mu_h \sim 10^{-3} \text{ cm}^2\text{V}^{-1}\text{s}^{-1}$. Both dissociated electrons and holes will drift towards opposite electrodes. No carrier accumulation exists in this device and $k_{ISC-PP}(B)$ can be ignored here. When $V < V_t$, the P- T_X quenching can be ignored since the density of free polarons is quite low. In Fig. 1(a), the MPC curves measured under zero bias is mainly from the B induced T_X increase through $k_{ISC-X}(B)$. The fitting result reveals that $k_{ISC-X}(B)$ is a HF effect following the non-Lorenze line shape. The positive MPC_{ISC-X} indicates that D_{N50} can be treated as “generation” limited device. When $V > V_t$, holes are injected into NPB layer and the P- T_X quenching process is activated. The emerged LF component corresponds to the magnetic field effect on k_q , which is a low field effect and has a Lorenze line shape. The fitting result, that the values of MPC_{ISC-X} and MPC_{TPQ} are both positive, is consistent with what we just discussed that both components are originate from the

increase of T_X density.

Since OMFES are universal phenomena in OSEs, the model based on B field induced increase of k_{ISC} and decrease of k_q conjectured from D_{N50} , should also apply to other OSE based devices. Thus we studied Alq_3 based device ITO/ Alq_3 (50 nm)/Mg:Ag (D_{A50}). Different from NPB, Alq_3 is usually used as an electron transporting and light emitting layer. The value of hole mobility is orders of magnitude lower than the electron mobility in Alq_3 , $\mu_e \sim 10^{-6} \text{ cm}^2\text{V}^{-1}\text{s}^{-2}$ and $\mu_h \sim 10^{-8} \text{ cm}^2\text{V}^{-1}\text{s}^{-1}$ (ref. 24). Because of its low mobility, the dissociated holes will accumulate near the M/OSE interface, and will decrease the exciton dissociation probability due to the Coulombic attraction. Therefore, the PC is mainly come from dissociated electrons and its following drift towards opposite electrode. Most of the holes contribute to PC through forming PPs with electrons near M/OSE interface. Since the PP forms near M/OSE interface, the $k_{ISC-PP}(B)$ will affect the MPC significantly. Increase of k_{ISC-PP} will convert more T_{PP} into S_{PP} , and effectively decreases the accumulated holes, because the singlet states recombine much more quickly. As a result of the decrease in hole accumulation, the exciton dissociation probability at M/OSE interface increases, resulting a positive MPC component. When $V < V_b$, P- T_X quenching can be ignored due to free polaron density is low. The MPC is a result of both $k_{ISC-PP}(B)$ and $k_{ISC-X}(B)$, with MPC_{ISC-PP} positive while MPC_{ISC-X} having both positive and negative components.

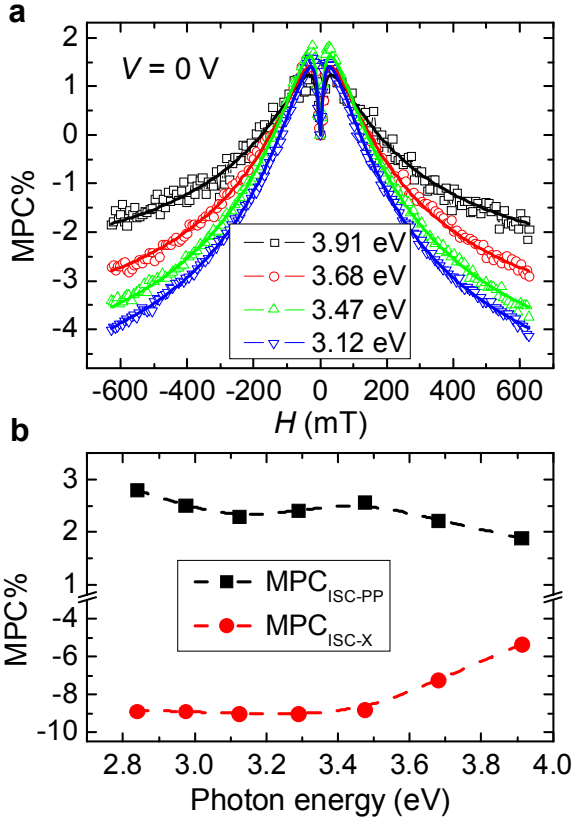


Figure 3 MPC of device ITO/ Alq_3 (50 nm)/Mg:Ag at zero bias. **a**, MPC curves measured with different excitation photon energies. The solid lines are fitting results using equation (5), with $B_{0LF} = 4.6$ mT and $B_{0HF} = 128$ mT, respectively. **b**, The fitting results of $MPC_{LF\infty}$ (MPC_{ISC-PP}) and $MPC_{HF\infty}$ (MPC_{ISC-X}) as a function of E_{hv} .

Figure 3(a) shows the E_{hv} dependent MPC curves of D_{A50} measured at zero bias. All the MPC curves consist of a LF positive component and a HF negative component. It is reasonable to assume that both MPC_{ISC-PP} and MPC_{ISC-X} in D_{A50} follow same line shape, a non-Lorenze type as in D_{N50} . The solid lines in Fig. 3(a) are fitting results using the following equation:

$$MPC(B) = \frac{MPC_{\infty LF} \cdot B^2}{(|B| + B_{0LF})^2} + \frac{MPC_{\infty HF} \cdot B^2}{(|B| + B_{0HF})^2} \quad (5)$$

with $B_{0LF} = 4.6$ mT and $B_{0HF} = 128$ mT. The fitting results of $MPC_{LF\infty}$ and $MPC_{HF\infty}$ as a function of E_{hv} are shown in Fig. 3(b). Obviously, that the LF and HF components correspond to MPC_{ISC-PP} and MPC_{ISC-X} , respectively. The fact, that $k_{ISC-X}(B)$ in Alq_3 is a HF effect and follows non-Lorenze line shape, is consistent with that in NPB. The negative value of MPC_{ISC-X} indicates that D_{A50} is “transport” limited at zero bias. As shown in Fig. 3(b), as E_{hv} decreases, MPC_{ISC-X} decreases and MPC_{ISC-PP} increases. This is because that, as E_{hv} decreases, relatively more light was absorbed in d1 and g2 region (Fig. 2(b)), enhancing the P- T_X scattering effect, and consequently the negative component of MPC_{ISC-X} . And this absorption region change also enhances the hole accumulation at M/OSE interface, making the $k_{ISC-PP}(B)$ effect more pronounced, increasing the positive MPC_{ISC-PP} value.

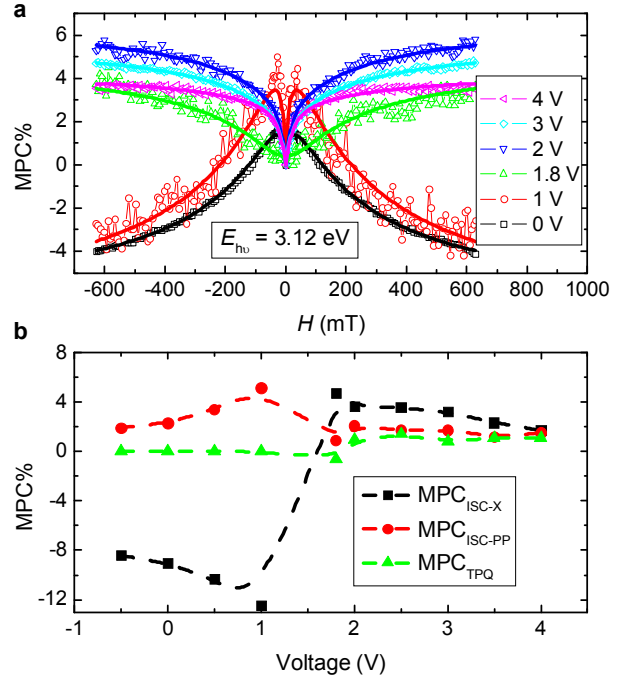


Figure 4 MPC of device ITO/ Alq_3 (50 nm)/Mg:Ag with $E_{hv} = 3.12$ eV. **a**, MPC curves measured at different bias conditions indicated. The solid lines are fitting results using equation (6), with $B_{0LF-PP} = 4.6$ mT, $B_{0HF-X} = 128$ mT and $B_{0LF-q} = 27$ mT, respectively. **b**, The fitting results of MPC_{ISC-PP} , MPC_{ISC-X} and MPC_{TPQ} as a function of applied bias.

In order to investigate the magnetic field effect on P- T_X quenching process in Alq_3 , V dependent MPC curves of D_{A50} with $E_{hv} = 3.12$ eV were also measured, and the results are

shown in Fig. 4(a). When $V < V_t$, MPC is dominated by LF positive MPC_{ISC-PP} and HF negative MPC_{ISC-X} . When $V > V_t$, carriers are injected and the P-T_X quenching is activated. Now the MPC consists of MPC_{ISC-PP} , MPC_{ISC-X} and MPC_{TPQ} . Based on that both the line shapes and field widths of MPC_{ISC-PP} and MPC_{ISC-X} should remain the same as those at zero bias conditions and the MPC_{TPQ} should have a Lorentze line shape and is a LF component the same as that in NPB, the observed MPC curves can be fitted using the following equation shown as solid lines in Fig. 4(a)

$$MPC(B) = \frac{MPC_{\infty LF-PP} \cdot B^2}{(|B| + B_{0LF-PP})^2} + \frac{MPC_{\infty HF-X} \cdot B^2}{(|B| + B_{0HF-X})^2} + \frac{MPC_{\infty LF-q} \cdot B^2}{B^2 + B_{0LF-q}^2} \quad (6)$$

with $B_{0LF-PP} = 4.6$ mT, $B_{0HF-X} = 128$ mT and $B_{0LF-q} = 27$ mT. The fitting result of $B_{0LF-q} = 27$ mT, indicating that the P-T_X quenching in Alq₃ is also a LF effect, consistent with that in NPB. The fitting values of MPC_{∞} for various components as a function of V were shown in Fig. 4(b). The MPC_{ISC-X} changed from negative to positive when the V crosses V_t . This is because that the e/h generation region/interface for exciton dissociation interchanged as V across V_t , enhancing the generation capability significantly due to energy compensation Δ increase, as shown in Fig. 2(e) and (f) which illustrate the case of $V < V_t$ and $V > V_t$ respectively. Then the positive component of MPC_{ISC-X} increases and D_{A50} cannot be treated as “transport” limited, resulting in the sign change.

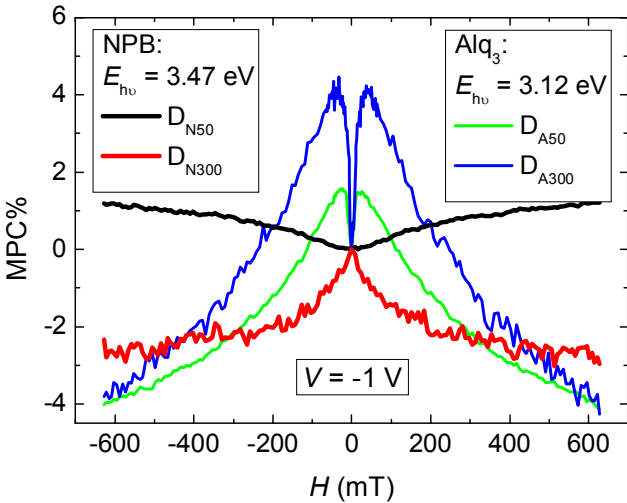


Figure 5 Comparison of MPC curves of devices with OSE layer thickness of 50 nm and 300 nm. For NPB based devices, E_{hv} is 3.47 eV and for Alq₃ based devices is 3.12 eV. For devices with 300 nm thick OSE layer, MPC curves were measured under a -1 V bias condition in order to reach a uniform electric field.

We have shown that although the measured MPC results are quite different between NPB and Alq₃ based devices, the underline magnetic field dependent physical processes are the same. The reason of the divergence between D_{N50} and D_{A50} is the difference in their device physics, such as energy bands alignment and carrier transport behaviors. In D_{A50} , it has been shown in “transport” limited case, MPC_{ISC-X} is negative. To further verify our model, we fabricates a NPB

based “transport” limited device, by simply increase the thickness of NPB layer to 300 nm (D_{N300}). Together an Alq₃ based device with the same thickness (D_{A300}) was also fabricated. It is expected from our analysis that in this NPB “transport” limited device, negative MPC_{ISC-X} should be observed, while in device D_{A300} , the signature of the line shape should be similar with that of D_{A50} . Figure 5 shows the MPC curves of D_{N300} and D_{A300} with $E_{hv} = 3.47$ eV and $E_{hv} = 3.12$ eV, respectively. Both were measured under $V = -1$ V bias condition, in order to achieve a uniform electric field. As can be seen in Fig. 5, the MPC value of D_{N300} is negative and dominated by a HF component, while the MPC curve of D_{A300} has similar line features with that of D_{A50} . This further confirms that the OMFES originate from the magnetic field induced increase of k_{ISC} and decrease of k_q and the device physics controls the sign change and the observed field dependence.

In conclusion, we have identified the underlying magnetic field dependent physical processes that are responsible for the observed OMFES. The ISC between singlet and triplet states is enhanced by an external magnetic field. It is revealed that the ISC between excitons is a high field effect, while that between polaron pairs is a low field effect. The P-T_X quenching is a low field effect and the quenching rate is reduced by an external magnetic field. It has been shown that the divergence of observed OMFES, such as sign changes and operating conditions dependences, originates from the changes in device physics. The result, that ISC-X is a high field effect and ISC-PP is a low field effect, reveals that magnetic field dependence of ISC is inversely proportional to the energy difference between singlet and triplet states. Although both can be treated as low field effect, the characteristic field width of TPQ process in Alq₃, ~27 mT, is apparently larger than that in NPB, ~8 mT. This implies that electron-T_X quenching and hole-T_X quenching have different magnetic field dependences. We believe that our result is benefit to further theoretical study of microscopic mechanism of OMFES.

Methods:

The 3×3 mm devices were fabricated on ITO patterned glass substrates. Before transferred into a vacuum chamber, the substrates were rigorously cleaned following by UV o-zone treatment. The organic layer and cathode electrodes were evaporated sequentially in a standard vacuum chamber with a base vacuum of 10⁻⁶ Torr. After fabrication the sandwiched structures, the devices were transferred to an inert N₂ atmosphere glove box and encapsulated. A Xe-lamp together with a Spex1681 spectrometer was used as the excitation source, and a standard lock-in technique was adopted to measure the photocurrent. The light was incident through the glass substrate and ITO. A HP4155A semiconductor parameter analyzer was used to measure the device current-voltage characteristics and as a constant voltage source. An electromagnet with field range from 0 to 800 mT was used to apply the magnetic field. All the measurements were conducted at room temperature. No magnetic field direction dependence was observed and the magnetic field was applied perpendicularly to the device current direction.

References

1. Forrest, S. R. The path to ubiquitous and low-cost organic electronic appliances on plastic. *Nature* **428**, 911-918 (2004).
2. Dediu, V. A., Hueso, L. E., Bergenti, I. & Taliani C. Spin routes in organic semiconductors. *Nature Mater.* **8**, 707-716 (2009).
3. Frankevich, E. L. *et al.* Polaron pair generation in poly(phenylene vinylenes). *Phys. Rev. B* **46**, 9320-9324 (1992).
4. Pope, M. & Swenberg, C. E. *Electronic Processes in Organic Crystals* (Clarendon, New York, 1999).
5. Kalinowski, J., Szmytkowski, J. & Stampor, W. Magnetic hyperfine modulation of charge photogeneration in solid films of Alq₃. *Chem. Phys. Lett.* **378**, 380-387 (2003).
6. Kalinowski, J., Cocchi, M., Virgili, D., Marco, P. D. & Fattori, V. Magnetic field effects on emission and current in Alq₃-based electroluminescence diodes. *Chem. Phys. Lett.* **380**, 710-715 (2003).
7. Mermer, Ö. *et al.* Large magnetoresistance in nonmagnetic π -conjugated semiconductor thin film devices. *Phys. Rev. B* **72**, 205202 (2005).
8. Shen, Y. *et al.* Hyperfine interaction and magnetoresistance in organic semiconductors. *Phys. Rev. B* **74**, 045213 (2006).
9. Hu, B. & Wu, Y. Tuning magnetoresistance between positive and negative values in organic semiconductors. *Nature Mater.* **6**, 985-991 (2007).
10. Xu, Z. & Hu, B. Photovoltaic processes of singlet and triplet excited states in organic solar cells. *Adv. Funct. Mater.* **18**, 2611-2617 (2008).
11. Bergeson, J. D., Prigodin, V. N., Lincoln, D. M. & Epstein, A. J. Inversion of magnetoresistance in organic semiconductors. *Phys. Rev. Lett.* **100**, 067201 (2008).
12. Davis, A. H. & Bussmann, Large magnetic field effects in organic light emitting diodes based on Alq₃/NPB bilayers. *K. J. Vac. Sci. Technol. A* **22**, 1885-1891 (2004).
13. Zhang, Y., Liu, R., Lei, Y. L. & Xiong, Z. H. Low temperature magnetic field effects in Alq₃-based organic light emitting diodes. *Appl. Phys. Lett.* **94**, 083307 (2009).
14. Desai, P., Shakya, P., Kreouzis, T. & Gillin, W. P. The role of magnetic fields on the transport and efficiency of aluminum tris(8-hydroxyquinoline) based organic light emitting diodes. *J. Appl. Phys.* **102**, 073710 (2007).
15. Wang, F. J., Bäessler, H. & Vardeny, Z. V. Magnetic field effects in π -conjugated polymer-fullerene blends: evidence for multiple components. *Phys. Rev. Lett.* **101**, 236805 (2009).
16. Majumdar, S. *et al.* Role of electron-hole pair formation in organic magnetoresistance. *Phys. Rev. B* **79**, 201202(R) (2009).
17. Bloom, F. L., Kemerink, M., Wagemans, W. & Koopmans, B. Sign inversion of magnetoresistance in space-charge limited organic devices. *Phys. Rev. Lett.* **103**, 066601 (2009).
18. Bobbert, P. A., Nguyen, T. D., van Oost, F. W. A., Koopmans, B. & Wohlgenannt, M. Bipolaron mechanism for organic magnetoresistance. *Phys. Rev. Lett.* **99**, 216801 (2007).
19. Yusoff, A. R. B. M., da Silva, W. J., Serbena, J. P. M., Meruvia, M. S. & Hümmelgen, I. A. Very high magnetocurrent in tri-(8-hydroxyquinoline) aluminum-based bipolar charge injection devices. *Appl. Phys. Lett.* **94**, 253305 (2009).
20. Lupton, J. M. & Boehme, C. Magnetoresistance in organic semiconductors. *Nature Mater.* **7**, 598-599 (2008).
21. Majumdar, S., Majumdar, H. S., Tobjörk, D. & Österbacka, R. Towards printed magnetic sensors based on organic diodes. *Phys. Status Solidi A* **206**, 2198-2201 (2009).
22. Hung, L. S. & Chen, C. H. Recent progress of molecular organic electroluminescent materials and devices. *Mater. Sci. Eng. R* **39**, 143-222 (2002).
23. Xiong, Z. H., Wu, D., Vardeny, Z. V. & Shi, J. Giant magnetoresistance in organic spin-valves. *Nature* **427**, 821-824 (2004).
24. Tse, S. C., Kwok, K. C. & So, S. K. Electron transport in naphthylamine-based organic compounds. *Appl. Phys. Lett.* **89**, 262102 (2006).
25. Li, J. *et al.* Highly efficient phosphorescent organic light emitting devices based on Re(CO)₃Cl-bathophenanthroline. *Semicond. Sci. Technol.* **22**, 553-556 (2007).
26. Zhang, S., Song, J., Kreouzis, T. & Gillin, W. P. Measurement of the intersystem crossing rate in aluminum tris(8-hydroxyquinoline) and its modulation by an applied magnetic field. *J. Appl. Phys.* **106**, 043511 (2009).
27. Peumans, P., Yakimov, A. & Forrest, S. R. Small molecular weight organic thin-film photodetectors and solar cells. *J. Appl. Phys.* **93**, 3683-3723 (2003).
28. Lebental, M. *et al.* E. Diffusion of triplet excitons in an operational organic light-emitting diode. *Phys. Rev. B* **79**, 165318 (2009).
29. Hill, I. G., Kahn, A., Soos, Z. G. & Pascal Jr., R. A. Charge-separation energy in films of conjugated organic molecules. *Chem. Phys. Lett.* **327**, 181-188 (2000).
30. Ghosh, A. K. & Feng, T. Merocyanine organic solar cells. *J. Appl. Phys.* **49**, 5982-5989 (1978).
31. Ern, V. & Merrifield, R. E. Magnetic field effect on triplet exciton quenching in organic crystals. *Phys. Rev. Lett.* **21**, 609-611 (1968).

Acknowledgements

This work was supported by the Research Grant Council of Hong Kong SAR government via grant number HKUST16/CRF/08 and HKU10/CRF/08.